Innovative Compact Coronagraph Approach for Balloon-borne Investigation of Temperature and Speed of Electrons in the corona (BITSE)

Qian Gong*, Natchimuthuk Gopalswamy, Jeffrey Newmark
NASA Goddard Space Flight Center, 8800 Greenbelt Road, Greenbelt, MD 20771 USA

ABSTRACT

We are developing an innovative compact coronagraph for studying the physical conditions in the solar wind acceleration region. This paper presents the new development of the compact coronagraph for the investigation of temperature and speed of electrons in the solar corona. The proposed compact coronagraph is a one stage externally occulted coronagraph without internal occulter or Lyot stop mask. The key of the new idea is to set the inner field cutoff at the External Occulter (EO) much smaller than the specified inner field cutoff. A second occulter on the surface of the detector array removes the remaining diffraction. The occulter on the detector surface functions similar to an internal occulter with the Inner Field of View Cutoff (IFoVC) exactly the same as specified. For BITSE, the desired inner field cutoff is 3 $R_\odot$, but the cutoff at EO is only 1.5 $R_\odot$. The diffraction analysis shows that in the sensor plane, the diffraction intensity at the 3 $R_\odot$ is not sensitive to the EO cutoff, either at 1.5 $R_\odot$ or close to 3 $R_\odot$. The advantage of having a smaller EO cutoff is that the vignetting decreased for the Field of View (FoV) near 3 $R_\odot$, therefore, the signal increases. Meanwhile, the diffraction of Point Spread Function is much less in the radial direction, which not only increases the image quality around 3 $R_\odot$, but also increases the encircled energy and signal to noise ratio. In other words, the data is useful right at 3 $R_\odot$! The BITSE optical design and diffraction analysis will be presented in detail. The simulation shows the signal to noise ratio obtained from the diffraction and vignetting data enables corona temperature and speed measurement.

Keywords: Compact solar coronagraph, diffraction compression, Polarization camera

1. INTRODUCTION

From science point of view, what differentiates BITSE to other coronagraph missions is that BITSE is to measure the coronal temperature and velocity, the other missions only measured the coronal density. The coronal temperature and velocity is measured based on the ratio of the density at selected wavelengths. Therefore, it requires a much higher SNR to extract more accurate temperature and velocity information. From an engineering point of view, BITSE has to be designed in such a way that it is able to provide required SNR.

The balloon mission is a low budget mission. The sky brightness due to balloon's flight height provides another challenge to the mission's science goal. We used a compact coronagraph with novel features to meet the challenge. The main difference of the compact coronagraph relative to the normal coronagraph is the following. The traditional externally occulted coronagraph usually has 3 stages [1 - 3], including External Occulter (EO), Internal Occulter (IO), and Lyot Stop (LS). The compact coronagraph has only one stage. It is known that in 3 stage coronagraph, the first stage is a telescope to collect the coronal signal and to form an EO image for inserting Internal Occulter (IO). The second stage is a field lens group to form an image of entrance aperture for placing a Lyot stop. The third stage is a relay lens group to relay the coronal image to the detector array. In the compact coronagraph only the first stage is kept, the other two additional stages are removed. These two additional stages are removed to make the coronagraph more compact and simpler. The concept of the compact coronagraph has been published more than a decade ago [4]. In recent years, GSFC has developed a compact coronagraph testbed and tested it using a solar simulator at High Altitude Observatory (HAO). The coronagraph

* qian.gong-1@nasa.gov phone 1 301 286-1490;

for Balloon-borne Investigation of Temperature and Speed of Electrons in the corona (BITSE) has been designed and built using the compact coronagraph concept. Furthermore, two unique novel features are added to this design:

1. An occulter disk is placed on the detector surface. This disk not only reduces the diffracted light, it also reduces the vignetting at the defined Inner Field of View Cutoff (IFoVC). The vignetting reduction makes the Point Spread Function (PSF) much smaller, so the valid corona data can start right at the IFoVC. The reason and analysis will be described in Section 4.
2. A polarization sensitive sensor is used to avoid a polarizer wheel mechanism. Furthermore, it allows us to take images of all polarization at the same time. It allow us to record the fast moving corona information at different polarization simultaneously, which increases the accuracy of the measurement in the time domain.

Because the focus of this paper is how the novel design raise the SNR without compromising diffraction compression, the polarization sensor will not be discussed.

This paper is organized as follows: Section 2 discusses the coronagraph optical design. Section 3 discusses the diffraction of the system and the advantage of adding an occulter disk right at the detector surface. Section 4 discusses system vignetting and how it effect the Signal to Noise Ratio (SNR). The vignetting in the coronagraph instrument is very different from normal optical system. We discuss how to minimize the vignetting to obtain maximum signal without further sacrificing the diffraction compression. In the final section 5, we provides a summary and a plan for future coronagraph study.

2. CORONAGRAPH OPTICAL SYSTEM DESIGN

Most of the astronomical instruments' requirements include: spatial resolution, throughput, encircled energy, etc. But for coronagraph, the most important one is how efficient it compresses the diffracted light from the Sun. The past solar coronagraph history shows that externally occulted coronagraph provides the best result for the interested region in 3 – 30$R_\odot$. BITSE's FoV, the solar wind acceleration region in 3 – 9 $R_\odot$, is within the region that externally occulted coronagraph provides the best performance. Therefore, it is selected for BITSE coronagraph.

What makes BITSE challenging is that it is not simply measure the coronal density, it needs to extract the information from density to create the temperature and velocity maps. N. Reginald, et al. has described how to obtain the temperature and velocity information from total solar eclipse of June 21, 2001 [5]. Compared to the occasional opportunity during total solar eclipse, BITSE is a demonstration of developing an instrument that could constantly monitor the temperature and velocity in the FoV that is further away from Sun. Using the method described in N. Reginald, 4 narrow bandpass filters are selected for BITSE. Besides, the aperture diameter has increased to 50mm to increase the SNR, which is larger than most of the coronagraph on orbit, such as, Solar and Heliospheric Observatory (SOHO)/Large Angle and Spectrometric Coronagraph (LASCO) C2 and C3, and SolarTerrestrialRelationsObservatory(STEREO)/SunEarthConnection Coronal and Heliospheric Investigation (SECCHI) COR1 and COR2. The optical specification derived from science goal is listed in Table 1.

Table 1. BITSE optical system specifications.

Parameter	**Range**
FOV (R_0)	15*
Inner FOV cutoff (R_0)	3
Wavelength range (nm)	380 – 430, including broadband
Effective Focal Length (mm)	103
Entrance pupil diameter (mm)	50

Detector array	CCD, 1950x1950, 7.4μm pixel**
Diffraction and vignetting	S/N ratio meets requirement based on science model
Optics Throughput (average over λ & FOV)	> 85% ***

The optical system is designed based on the specification above. The BITSE optical system layout and standalone lens group are shown in Figure 1 and 2.

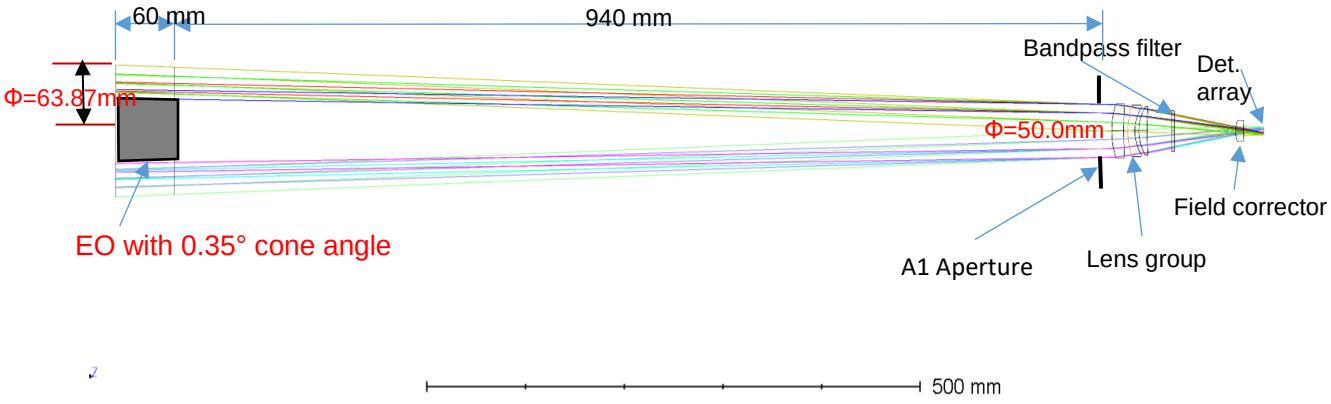

Figure 1. BITSE optical system layout. The EO diameter and cone angle of EO is optimized to best compress the diffraction at 1.5 $R_\odot$ in order to decrease the beam vignetting nearby IFoVC, even though the specified IFoVC is 3.0 $R_\odot$. The 3.0 $R_\odot$ occulter mask is attached to the detector array. The advantage in SNR of this kind of design will be addressed in Sections 3 and 4. The long distance between EO and lens group is also for decreasing the beam vignetting and increasing the SNR to compensate the noise caused by the sky brightness at the balloon flight height ~120,000 ft.

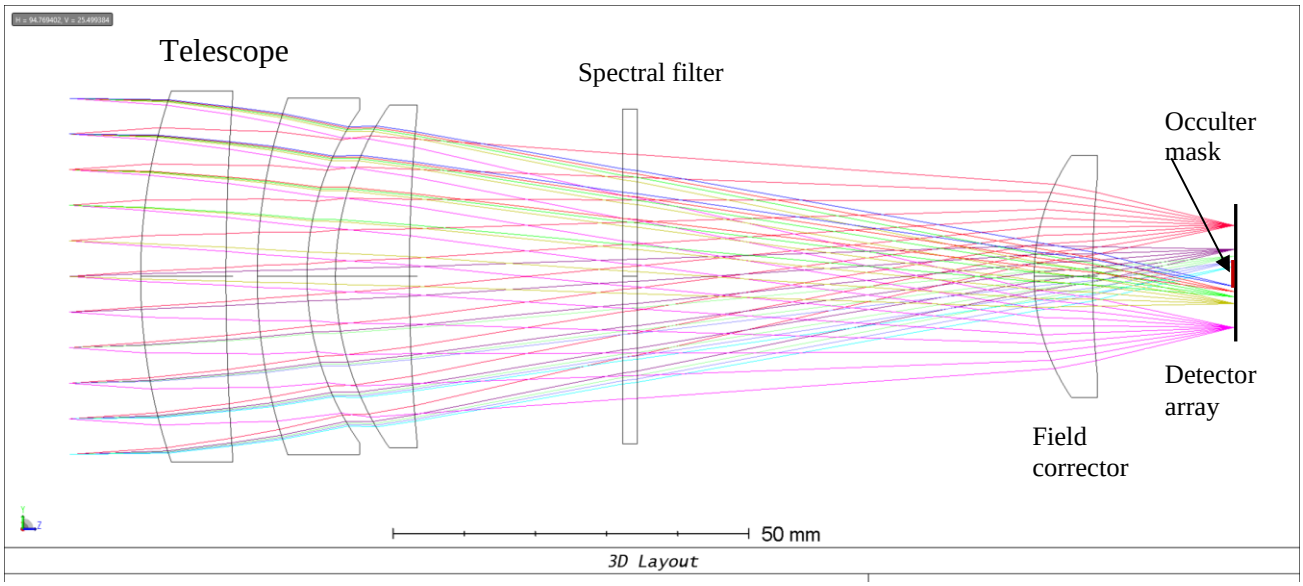

Figure 2. Standalone lens group design. The main part of the lens group is a telescope to image the solar corona on the detector. The first 3 lenses are the telescope body. The spectral filter(s) is behind between the telescope and the field corrector lens. The occulter mask with 3.0 $R_\odot$ cutoff is attached to the detector chip.

As mentioned above, the goal of this balloon mission is to measure the temperature and velocity of the solar corona. Therefore 4 narrowband spectral filters are needed [5]. The 4 filters are mounted to a wheel mechanism. Each filter is rotated into the optical path sequentially. The peak wavelengths are 393.5nm, 398.7nm, 405.0nm, and 423.3nm. We also have a filter with a broader bandwidth from 380m to 450nm to image the corona density. Because all wavelength bands are in near UV, the special attention was paid to select lens glasses with high transmittance in the selected wavelength range. The image quality is great as shown in the spot diagram (Figure 3).

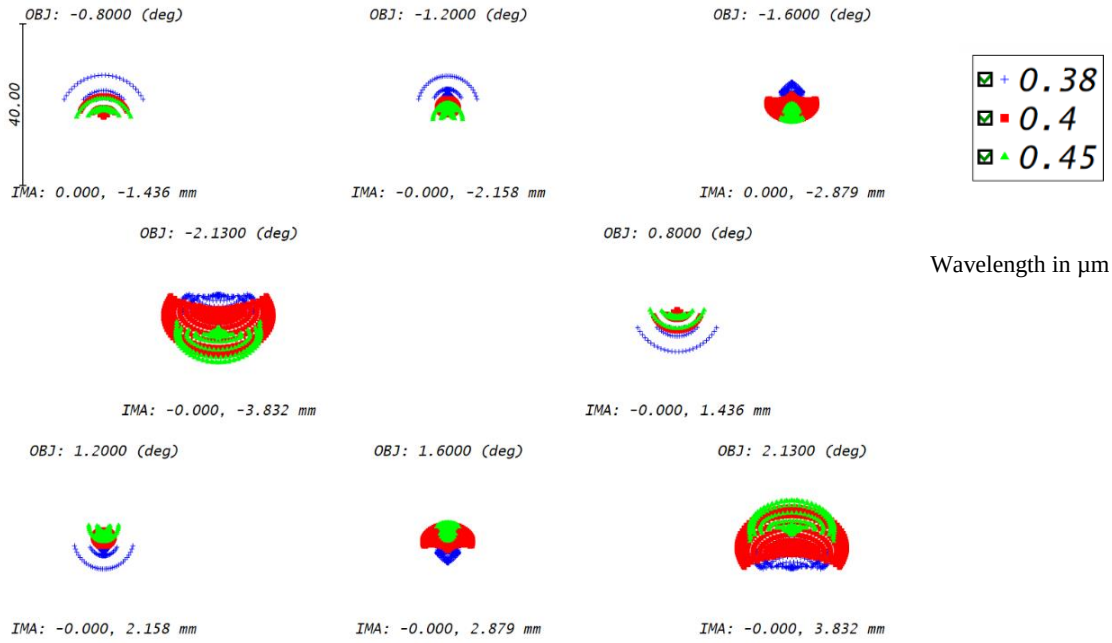

Figure 3. Spot diagram of the coronagraph at different FoV. Each color in the diagram presents a different wavelength shown on the right. Most of the time during the mission, one narrowband filter is used, which is equivalent to the spot with one color. The spot size meets the specification. Actually, we even need to defocus a little to cover a super pixel that includes 4 regular pixels with 4 different polarizations in 0°, 45°, 90°, and 135°.

3. CORONAGRAPH DIFFRACTION COMPRESSION

In the coronagraph field, it is the common knowledge that diffraction is one of the most important criterions to evaluate performance. Based on BITSE specification, the wavelength range for narrowband filters is ~390 – 425 nm, therefore λ = 400nm is selected for the diffraction analysis.

As mentioned briefly in the introduction section, the novel portion of this design is to make the EO cutoff far less than the specified 3.0 $R_\odot$ at 1.5 $R_\odot$, and to place a small occulter disk on the center of detector array to cut the rest. This has differentiated it from the traditional conception that EO cutoff should be as close as the specified IFoVC. For a 3-stage coronagraph, EO should only leave the margin for IO and Lyot stop cutoff, and for the compact 1-stage coronagraph, it should be right at the specified IFoVC. The advantage of this arrangement greatly reduces the vignetting around IFoVC, because the small occulter disk at the image plane does not cut any corona signal beyond the required IFoVC. Combined with much smaller PSF, a big improvement has been made for increasing the signal. However, a question comes out: if this small EO increase the diffraction brightness to cancel the advantage brought by signal increase? To answer the question, a diffraction bright distribution has been simulated for 5 different EO at 1.0 $R_\odot$, 1.5 $R_\odot$, 2.0 $R_\odot$, 2.5 $R_\odot$, and 3.0 $R_\odot$. A Fast Fourier Transform (FFT) based wave propagation software, GLAD, was used for this simulation. A large

array size (16384 × 16384) has been used to avoid alias. The geometric parameters used in the simulation can be found in Figure 1. The EO is a 0.35° truncated cone with equally spaced fine grooves on the cone surface shown in Figure 4. It is also called multithreaded EO in some literatures [6]. The EO diameters for different EO cutoff is listed in Table 2. The occulter disk on the detector was not modelled in the simulation, because it is in the image plane, and any diameter can be used to block the area with the strongest diffraction intensity depending upon the applications.

Table 2. EO diameters at 5 different IFoVC angles using BITSE coronagraph geometry.

IFoVC (R⊙)	1	1.5	2	2.5	3
Front dia. (mm)	59.49	63.87	68.26	72.64	77.02
Back dia. (mm)	58.76	63.14	67.52	71.90	76.28

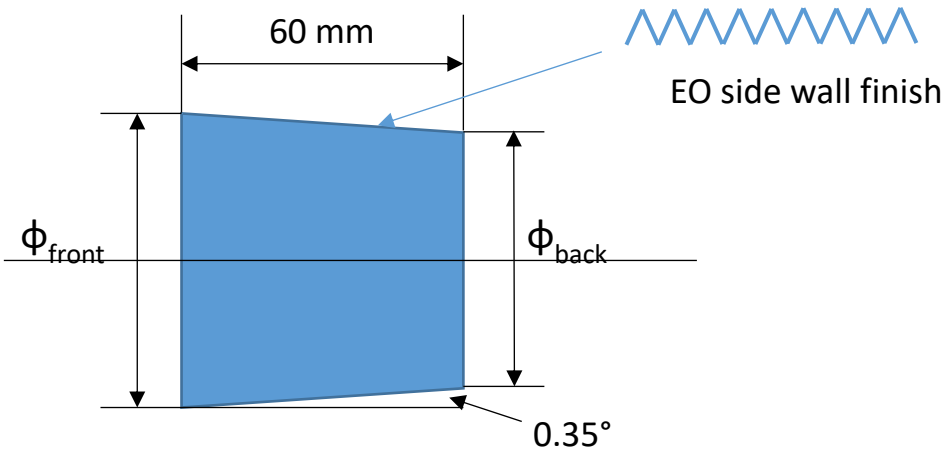

Figure 4. EO geometry. The diameters ϕ_{front} and ϕ_{back} are listed in Table 4. The optimized cone angle is 0.35°, which is very close to the 40' (0.33°) cone angle M. Bout, et al presented in [6]. The side wall finish is equally spaced grooves with saw tooth profile.

During the diffraction simulation, 5 SECCHI COR2 [2] like disks are used to simulate the external occulter cone, which is about factor of 2 less efficient than the cone with fine groove finish [6]. The result is quite interesting. The diffraction brightness is independent of EO cutoff beyond the cutoff point except for the cutoff at 1.0 $R_\odot$ where the diffraction brightness is higher than the rest. The simulation result is plotted in Figure 5. This discovery is significant for the single stage coronagraph design. It indicates that if we can add a mask on the image plane to block the area within the specified IFoVC, we are able to decrease the vignetting dramatically near the specified IFoVC without compromising the diffraction compression. This will increase the SNR considerably to provide enough SNR to measure the corona temperature and velocity right at the specified 3.0 R⊙. In comparison, the traditional coronagraphs starts the useful range at least 0.5 R away from the specified IFoVC.

Based on the result in Figure 5, the EO cutoff for BITSE is selected at $1.5R_\odot$ to minimize the vignetting and maximize the SNR. This is because the smaller the EO cutoff is, the less the vignetting close to specified IFoVC. In the next section, the SNR versus the vignetting will be detailed. Here we just simply mention that the noise introduced by the diffracted light is dominated by photon noise that is proportional to $\sqrt{n_d}$, where n_d is the number of photons created by diffraction. However, the number of signal photons n_c due to reduced vignetting is proportional to n_c linearly. That is, $n_c = 10$ is to cancel $n_d = 100$. Even more, the n_d is unchanged here, so a pure signal gain is achieved by reducing EO cutoff and place an occulter disk on the detector chip. Figure 6 shows the diffraction brightness distribution in the image plane.

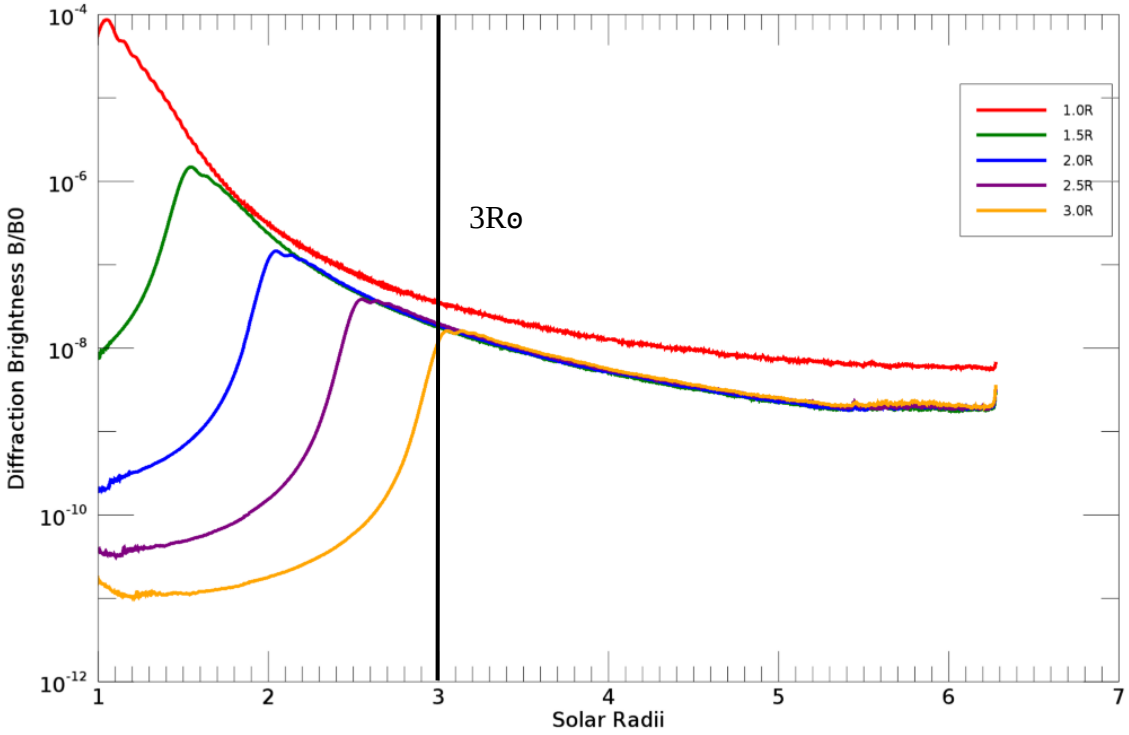

Figure 5. Normalized Diffraction brightness ($B/B_{\odot}$) versus solar radii in log scale. The black vertical line is the specified IFoVC at $3.0R_{\odot}$. The other curves are the diffraction brightness at different EO cutoff. Except EO cutoff at 1.0 $R_{\odot}$, all other cutoff does not change the diffraction distribution beyond the specified $3.0R_{\odot}$.

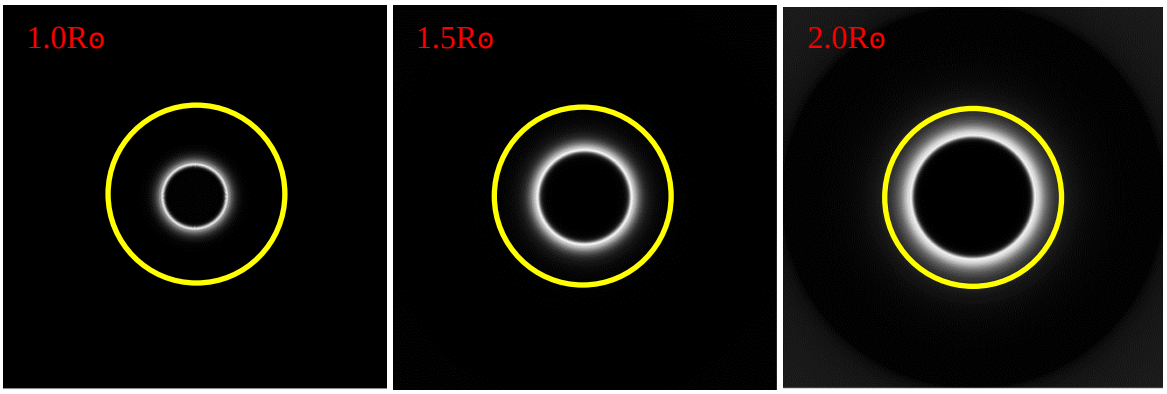

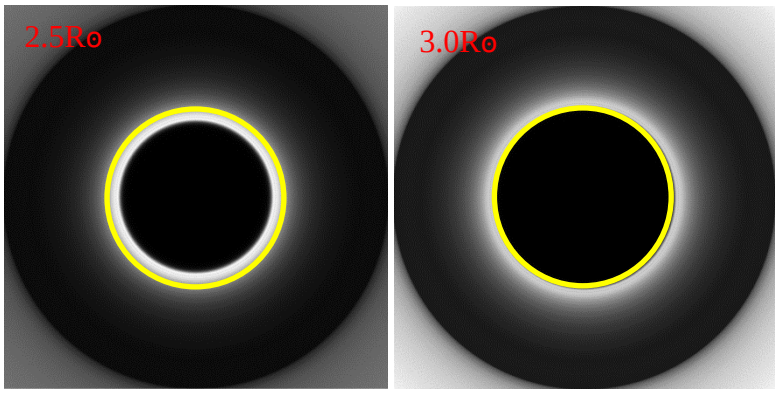

Figure 6. Diffraction intensity distribution in the image plane. The distributions are for EO cutoff at 1.0, 1.5, 2.0, 2.5, and 3.0 Rʘ, respectively. The yellow circles indicate the 3.0Rʘ FoV in the image plane. Note that the images are normalized to its own maximum. To obtain the relative diffraction brightness, the values in Figure 5 need to be multiplied. EO cutoff at 1.5 Rʘ is the selection of BITSE. The image is in linear scale.

Besides the vignetting, the new design has 2 other advantages from instrument engineering point of view:

1. It relaxes EO/telescope alignment tolerance. Use the Figure 6 as an example, if EO cutoff is 2.0Rʘ or smaller, the diffraction ring is far enough from diffraction edge. The moderate alignment error wouldn't let the diffraction rings that are leaked into the system to cause CCD array's saturation. The only effect can be seen is a slight offset of FoV.
2. The cleanliness requirement and EO fabrication tolerance can be relaxed too. This is because of the edge diffraction due to EO edge is masked off by the occulter disk on the detector. So the imperfectness of the EO or dust particles on the EO becomes less critical to the coronagraph image on the detector.

4. VIGNETTING AND PSF NEAR INNER FIELD OF VIEW CUTOFF

In the last section, we have pointed out that this innovated compact coronagraph design decreases the beam vignetting caused by EO without compromising the diffraction compression capability. This section discusses the relation between EO cutoff and the percentage of unvignetted beam using the 5 EO cutoff cases from the last section. The vignetting analysis is performed in Zemax, which is a commercial lens design software. The same coronagraph design shown in Figure 1 and the same EO diameters listed in Table 2 are used for this analysis. The percentage of the unvignetted rays at different EO cutoff is plotted in Figure 7.

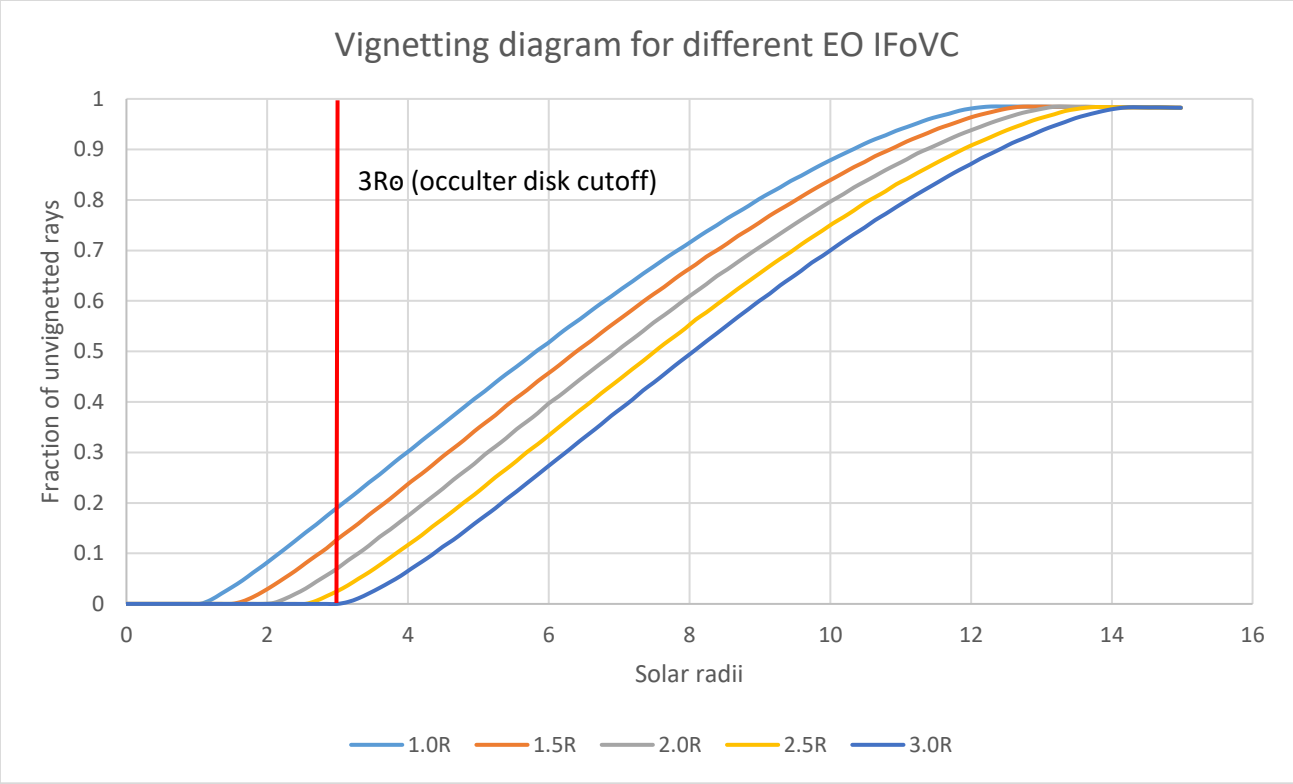

Figure 7. Vignetting diagram versus FoV for different EO cutoff from 1.0 Rʘ to 3.0 Rʘ. The vertical red line is at 3.0 Rʘ.

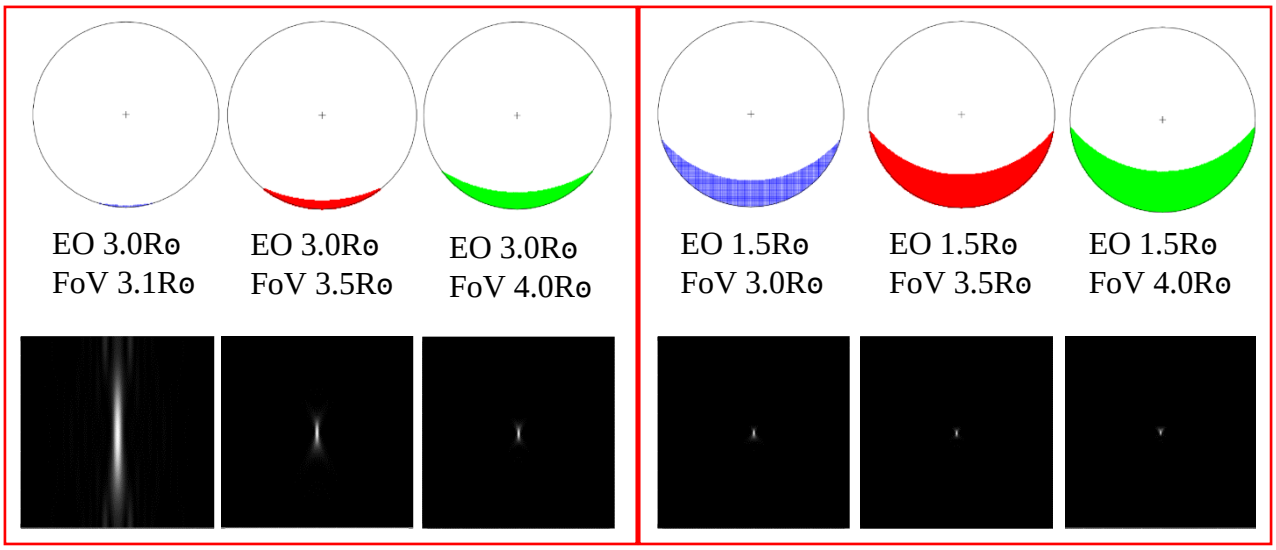

Figure 8. PSF comparison for EO cutoff at 3.0Rʘ and 1.5Rʘ. The left 3 pairs are the beam footprints and corresponding PSF's for EO cutoff at 3.0Rʘ. The right 3 pairs are for EO cutoff at 1.5Rʘ. The top row is the beam footprints at A1 aperture to display the vignetting at different FoV, and the bottom row is the PSFs corresponding to the vignetted footprints. For both EO cutoffs, the FoVs are near the IFoVC at 3.0Rʘ, 3.5 Rʘ, and 4.0Rʘ, except FoV 3.0Rʘ for EO cutoff at 3.0Rʘ is replaced with 3.1Rʘ because there is no rays getting through A1 aperture at FoV = 3.0Rʘ.

It is seen that the fraction of unvignetted rays is ranged from 0 for EO cutoff at 3.0 R⊙ to about 20% at 1.0 R⊙. From reducing vignetting point of view, it is best to have EO cutoff at 1.0R⊙. However, the diffraction for EO at 1.0R⊙ is higher. Besides, it is riskier to have EO at 1.0 R⊙, because the alignment tolerance is tighter, and any pointing error will let direct sun light leak into the coronagraph through aperture A1. That is the reason that BITSE selected the EO cutoff at 1.5 R⊙. In the most interested solar wind active region from 4 R⊙ to 8 R⊙, the unvignetted signal rays increase more than 15% for having EO cutoff at 1.5R⊙.

In addition to reducing the vignetting and raising the signal level, the less vignetting means a larger footprint at the pupil plane. It is known that for a system with a fixed focal length, the larger the footprint, the smaller the PSF is. The smaller PSF concentrates the signal in a smaller number of detector pixels. For the signal, fast moving K corona due to Thompson scattering, the spatial resolution and shorter exposure time is necessary. The smaller PSF is required to capture the K corona structure and retrieve the temperature and velocity information from it. Figure 8 shows the footprints at A1 aperture and the corresponding PSF in the image plane.

It is noted that the PSF at FoV of 3.0R⊙ for EO cutoff at 1.5R⊙ is already better than that the FoV at 4.0R⊙ for EO cutoff at 3.0R⊙, which quantitatively illustrates that the innovative BITSE coronagraph does provide higher signal without compromising the diffraction compress. It also illustrates that the BITSE coronagraph could provide corona data right at the IFoVC of 3.0R⊙ with a good quality images. This has been approved by the BITSE spatial resolution test in the lab, which will be published in another paper soon.

SNR is more complicated. Not only is diffracted light considered a noise to signal, the Thompson scattering radiated K-corona, but F-corona caused by dust particle scattering is also a noise source to the signal K-corona. However, F-corona is beyond our control, so we just compare the percentage of ray increase for EO cutoff at 3.0R and at 1.5R⊙ relative to diffracted light at 3 FoV = 3.1, 3.5, and 4.0 R⊙. The figure 5 shows that the diffracted light for EO cutoff at 1.5 and 3.0 R⊙ is the same, so the improvement is from two factors – vignetting and PSF size. The vignetting and relative image size versus FoV for the two cases are listed in Table 3.

Table 3. Fraction of unvignetted rays and corresponding PSF at different FoV nearby IFoVC for the two EO cutoffs

	Fraction of unvignetted rays			Relative PSF size		
	3.1R⊙	3.5R⊙	4.0R⊙	3.1R⊙	3.5R⊙	4.0R⊙
EO cutoff 1.5R⊙	0.138	0.18	0.235	0.018269	0.010769	0.008462
EO cutoff 3.0R⊙	0.0015	0.023	0.065	1	0.074038	0.030288

The PSF size in Table 3 is an estimate. It counts for the number of pixels to 1/e of the peak, then normalized to the pixel number of maximum size. If we define ξ = the fraction of unvignetted rays divided by the PSF size as the signal strength measure, the improvement ratio of EO cutoff at 1.5 R⊙ to EO cutoff at 3.0 R⊙ can be written as $\xi_{EO1.5} / \xi_{EO3.0}$. The improvement ratio is listed in Table 4.

Table 4. $\xi_{EO1.5}$, $\xi_{EO3.0}$ and improvement ratio at 3 FoV.

	3.1R⊙	3.5R⊙	4.0R⊙
ξ (EO 1.5R⊙)	7.553684	16.71429	27.77273
ξ (EO 3,0R⊙)	0.0015	0.310649	2.146032
Improvement ratio	5035.789	53.80435	12.94143

Table 4 shows that the improvement ratio is a function of FoV. When the FoV is close to the IFoVC 3.0 R⊙, the improvement ratio is huge. With the FoV moving away from IFoVC, the improvement ratio getting smaller and smaller. Eventually, the PSF difference can be ignored, the improvement ratio is settled with the ratio of unvignetted rays, which is ~1.33 at FoV = 9.0R⊙ for BITSE coronagraph. This improvement ratio implies that the corona signal is useable right at IFoVC 3.0 R⊙. Even at 4.0R⊙, the improvement factor is still more than an order of magnitude better, which is a substantial boost to SNR nearby IFoVC.

5. SUMMARY

This paper has demonstrated that we have found a way to increase the SNR without compromising diffraction compression. The innovated compact coronagraph reduces the EO cutoff and places an occulter disk at the specified IFoVC. It has significantly increased SNR nearby the specified IFoVC. Even though the FoV nearby the IFoVC benefits most from the invention, the SNR increase does not stop until the completely unvignetted FoV is reached. The SNR increase drops when FoV moves away from the IFoVC. Compared to traditional coronagraphs, even though both coronagraphs claim 3.0R cutoff, the traditional one can only get the useful corona data start from 3.5 or 4.0R. But our data is useful right at 3.0R. This advantage enables us to investigate the temperature and velocity of the solar corona beyond corona density.

BITSE coronagraph has been designed using this concept. It has gone through alignment and lab test stages. It is currently being integrated to the gondola and get ready for a balloon flight in late August or early September. Even though the sky brightness at the balloon altitude is not ideal and the flight time is limited, we still expect to see the corona temperature and velocity at reduced spatial resolution. The lab test results and balloon flight results will be presented in another paper shortly.

REFERENCES

[1] Editors: Fleck, Bernhard, Domingo, Vicente, Poland, Arthur I. (Eds.) [The SOHO Mission], Springer Netherlands, (1995). ISBN 978-94-009-0191-9

[2] Editor: C. T. Russell [The STEREO Mission], Springer, 83-88, (2008). ISBN-978-0-387-09648-3

[3] A. Howard, J. D. Moses, A. Vourlidas, J. S. Newmark, D. G. Socker, S. P. Plunkett, C. M. Korendyke, J. W. Cook, A. Hurley, J. M. Davila, W. T. Thompson, O. C. St. Cyr, E. Mentzell, K. Mehalick, J. R. Lemen, J. P. Wuelser, D. W. Duncan, T. D. Tarbell, C. J. Wolfson, A. Moore, R. A. Harrison, N. R. Waltham, J. Lang, C. J. Davis, C. J. Eyles, H. Mapson-Menard, G. M. Simnett, J. P. Halain, J. M. Defise, E. Mazy, P. Rochus, R. Mercier, M. F. Ravet, F. Delmotte, F. Auchere, J. P. Delaboudiniere, V. Bothmer, W. Deutsch, D. Wang, N. Rich, S. Cooper, V. Stephens, G. Maahs, R. augh, D. McMullin, and T. Carter, "Sun Earth Connection Coronal and Heliospheric Investigation (SECCHI)," Space Sci. Rev. 136, 67-115 (2008)

[4] Qian Gong and Dennis Socker, "Theoretical study of the occulted solar coronagraph", Proceedings Volume 5526, Optical Systems Degradation, Contamination, and Stray Light: Effects, Measurements, and Control; (2004). https://doi.org/10.1117/12.549275

[5] Nelson L. Reginald, O. C. St. Cyr, Joseph M. Davila, and Jeffrey W. Brosius, "Electron Temperature and Speed Measurements in the Low Solar Corona: Results from the 2001 June E", The Astrophysical Journal, 599:596–603, (2003)

[6] M. Bout, P. Lamy, A. Maucherat, C. Colin, and A. Llebaria, "Experimental study of external occulters for the Large Angle and Spectroscopic Coronagraph 2: LASCO-C2", Appl. Opt., vol. 39, 3955–3962, 2000.